Supporting Information

Improving Needleless Electrospinning Throughput by Tailoring Polyurethane Solution Properties with Polysiloxane Additives

Kamran Iranshahi[1,2], Jean Schoeller[1,3], Nicolas Luisier[1], Michael Chung[4], Sina Hashemizadeh[5], Giuseppino Fortunato[1], Thijs Defraeye[1], René M. Rossi[1,3*]

[1]*Empa, Swiss Federal Laboratories for Materials Science and Technology, Laboratory for Biomimetic Membranes and Textiles, Lerchenfeldstrasse 5, CH-9014 St. Gallen, Switzerland*

[2]*ETH Zürich, Department of Environmental Systems Science, 8092 Zürich, Switzerland*

[3]*ETH Zürich, Department of Health Science and Technology, 8092 Zürich, Switzerland*

[4]*School of Engineering, The University of Edinburgh, King's Buildings, Mayfield Road, Edinburgh EH9 3JL, United Kingdom*

[5]*Foundation for Research on Information Technologies in Society (IT'IS), Zeughausstrasse 43, CH-8004 Zurich, Switzerland*

** Corresponding author's email: Rene.Rossi@empa.ch*

1. Solution characterization

Solution properties were measured experimentally and used as inputs to our mathematical models. The molecular weight was measured using gas permeation chromatography (GPC). The average molecular weight was 279 g mol^{-1}, and the polydispersity index was 1.02.

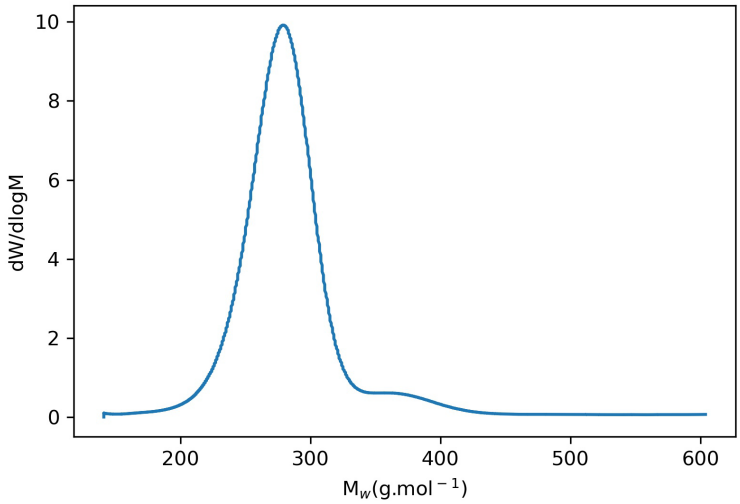

Figure S1 GPC chromatogram obtained for the PDMS-OH used in this study.

The emulsion status after vigorous shaking was followed using an optical camera. The following pictures (Figure S2) show the stability of the emulsions over 24h. As observed, the two solutions are immiscible and form an emulsion that stays stable over 24 h. Therefore, we believe it is safe to assume that the solution remains stable throughout the electrospinning process and no phase transition occurs throughout the process. The emulsions prepared were heterogeneous, and the measured solution properties do not refer to the bulk solution properties.

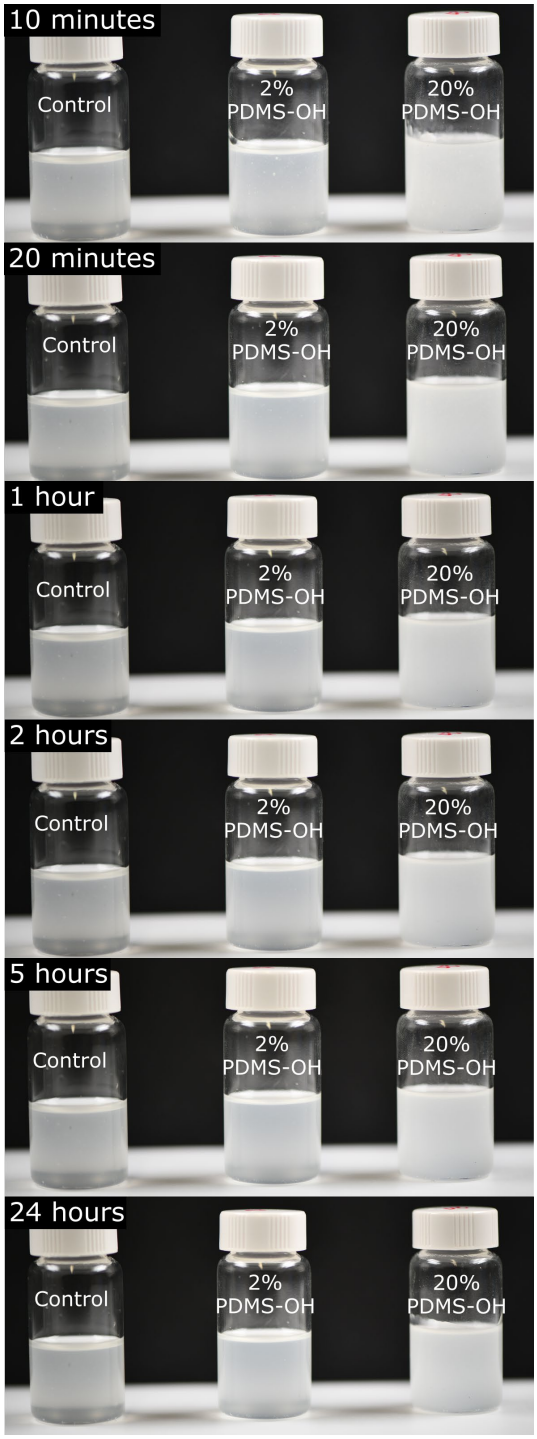

Figure S2 Stability of the emulsion over the span of 24h measured by the optical camera for 14.5% PUR solution (Control), with 2% and 20% PDMS-OH.

Solution properties are the primordial parameters influencing the electrospinning process and its throughput for the constant operating conditions. These properties include the contact angle on steel, conductivity, surface tension, and zero-shear viscosity.

Table S1 Composition, properties and entrainment of electrospun solutions.

Additive	Surface tension (mN/m)	Conductivity (µS/cm)	Contact angle on steel (°)	Zero-shear Viscosity (Pa*s)
-	35.43 ± 1.08	0.655 ± 0.007	44.3 ± 0.7	2.63
2 % PDMS-OH	21.82 ± 0.01	0.645 ± 0.006	38.1 ± 1.7	2.79
5 % PDMS-OH	21.36 ± 0.09	0.640 ± 0.018	34.2 ± 2.1	2.68
9 % PDMS-OH	21.57 ± 0.02	0.624 ± 0.015	31.6 ± 0.9	3.07
11 % PDMS-OH	21.06 ± 0.04	0.633 ± 0.002	32.1 ± 0.6	3.11
20 % PDMS-OH	20.83 ± 0.09	0.638 ± 0.007	29.0 ± 0.8	3.91
2 % octamethyltrisiloxane	34.68 ± 0.49	0.727 ± 0.027	37.5 ± 0.6	2.98
2 % PDMS-H	23.16 ± 0.14	0.732 ± 0.017	33.5 ± 0.2	3.01
2 % PDMS-HCH3	29.90 ± 0.31	0.977 ± 0.020	36.8 ± 0.1	3.03
2 % high MW PDMS-OH	25.57 ± 0.31	0.597 ± 0.011	37.8 ± 1.8	3.33
0.2 % TEAB	35.91 ± 0.61	64.26 ± 0.730	41.4 ± 1.7	2.18

In order to understand the influence of the solution rheological properties on the electrospinning behavior, flow curves were recorded on a rotational rheometer.

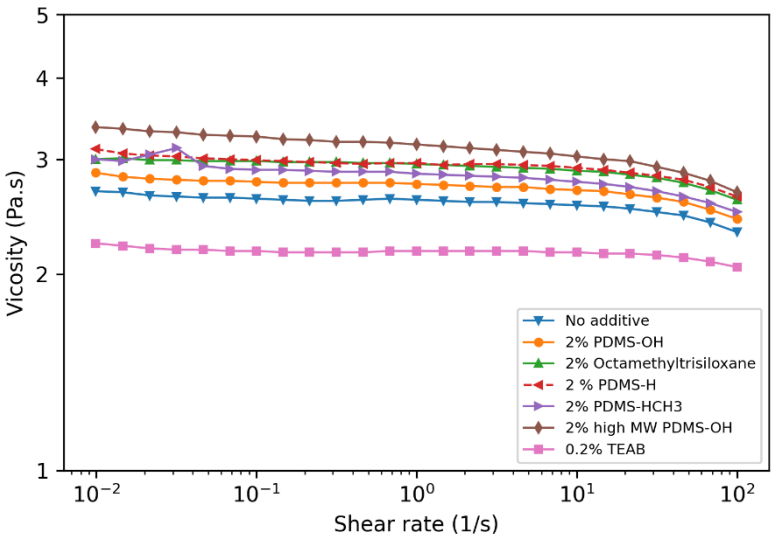

Figure S3 Flow curve of polyurethane solutions with different additives.

2. Physics-based computational model

The physics-based model aims to capture the static electric field inside the solution deposited on the wire. To model these process, the electrostatic potential field and ion charge transport under the high-voltage field are simulated. The specific physics and corresponding equations are described in the following paragraphs.

The electrical potential $\boldsymbol{V}$ [V] is linked to the electric field intensity $\boldsymbol{E}$ [V m^{-1}] by Eq.(S1). $\boldsymbol{E}$ is described by Poisson's equation, Eq.(S2):

$$\boldsymbol{E} = -\boldsymbol{\nabla} V \tag{S1}$$

$$\boldsymbol{\nabla}.(\varepsilon_0 \varepsilon_r \boldsymbol{E}) = \rho_e \tag{S2}$$

where $\boldsymbol{\nabla}$ and $\boldsymbol{\nabla}.$ indicate gradient and divergence operations, respectively. ρ_e [mol m^{-3} or C m^{-3}] is the space charge density (SCD) of the ion/fluid medium, ε_0 [C V^{-1} m^{-1}] is the dielectric permittivity of vacuum (8.854×10^{-12} C V^{-1} m^{-1}), and ε_r is the relative permittivity of the solution. Note that in this paper, inner product between vectors is denoted by point (for instance **A**.**B**). The ion transport is described by the continuity (i.e., convection-diffusion) equation for current density in the drift region (Ohm's law):

$$\boldsymbol{\nabla}.\boldsymbol{J} = 0 \tag{S3}$$

$$\boldsymbol{J} = \mu_e \rho_e \boldsymbol{E} - D_i \boldsymbol{\nabla} \rho_e \tag{S4}$$

where $\boldsymbol{J}$ [C m^{-2} s^{-1}] is the electric current density, μ_e [m^2 V^{-1} s^{-1}] is the ion mobility in the air (1.8×10^{-4} m^2 V^{-1} s^{-1}), and D_i [m^2 s^{-1}] is the diffusivity of the ions in the solution. In the particular case of charged particles (i.e., not considering neutral particles), the drift motion produced by the electric field (first term on the right-hand side of Eq.(S4)) is typically dominant, causing the equation to reduce to:

$$\boldsymbol{J} = \mu_e \rho_e \boldsymbol{E} \tag{S5}$$

The computational system configuration in this study has a 2D geometry, consisting of two wires as the emitter and collector electrodes with a distance of 25cm, and a rectangle with a dimension of L× 2h on the emitter wire as the solution (Figure S4). L and h are the wire length and the average thickness of the entrained solution on the wire, respectively. We applied a positive high voltage to the wire emitter (V=+60 kV with ρ_e=6×10^{-4} mol m^{-3}) and negative voltage to the collecting electrode V=-10 kV with ρ_e=0 mol m^{-3}. The temperature T_{ref} and relative humidity RH_{ref} were considered as 22℃ and 20% at the inlet. These are the controlled conditions for electrospinning in our experiments. Other simulation conditions, as well as the computational model, are summarized in Figure S4.

This model was implemented in COMSOL Multiphysics (version 5.4a). A fully-coupled direct solver, based on the MUMPS (MUltifrontal Massively Parallel sparse direct Solver) algorithm, was used for this simulation. The convergence threshold and other solver settings were determined based on sensitivity analysis in such a way that increases the tolerance further did not alter the solution results anymore. Mesh sensitivity analysis was also carried out to ensure that grids were built properly for the air and fruit domains. To this end, we increased the resolution of the grids until the results did not change anymore.

The grid consists of tetrahedral and quadrilateral finite elements which were refined toward electrode boundaries and the air–tissue interface for numerical accuracy enhancement.

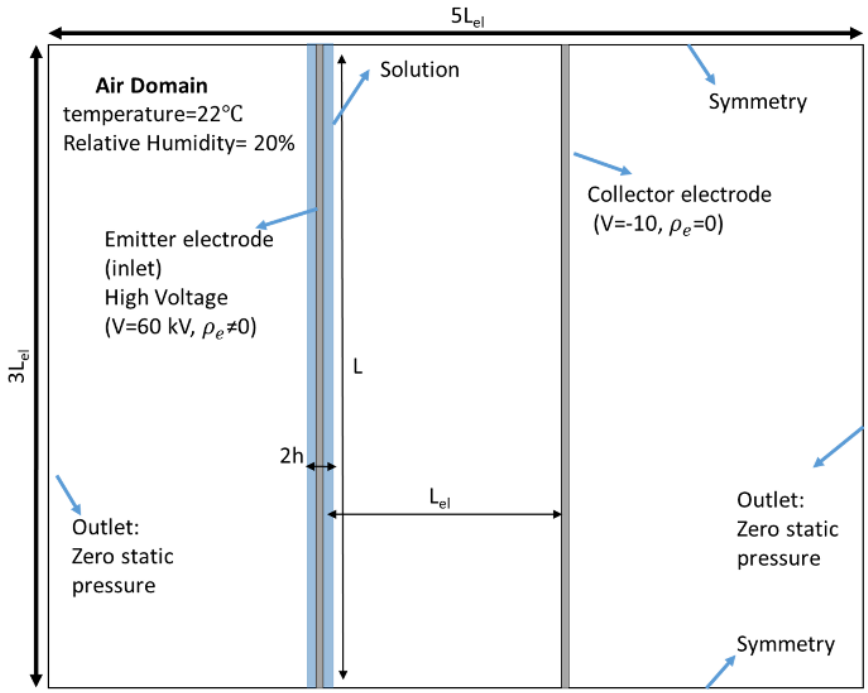

Figure S4 Computational model and simulation conditions (figure not to scale)

3. The dielectric relaxation spectroscopy

The dielectric relaxation spectroscopy was performed with the open coaxial probes (OCP) method [1]. We used the advanced implementation of the OCP probes and solvers of SPEAG (Schmid & Partner Engineering AG, Switzerland), namely the high precision DAK 3.5 200 MHz– 20 GHz probe in combination with a ZVA 67 (Rohde & Schwarz) vector network analyzer. The standard 3-point, Open, Short, and Load (de-ionized) calibration was performed prior to each measurement session [2,3]. The uncertainty of the measurement (Table S1) were established according to [1] that includes possible systematic errors due to design, calibration uncertainties, temperature differences between the calibration and measurements, and VNA noise.

As the extraction of the complex dielectric from the complex reflection coefficient, S11; is based on a full-wave analysis of Maxwell's equations in cylindrical geometry for semi-infinite samples, the influence of possible extra reflection from the sample boundaries of the finite configurations was examined by moving the sample with respect to the open coaxial probe. No change was observed in the measured S11 within the measurement uncertainty budget.

Table S2 Measurement incertitude of the dielectric relaxation spectroscopy measurements

	DAK-3.5	
Freq (GHz)	Δε (rel.)	Δσ (rel.)
0.2	1.7%	2.7%
0.3	1.7%	2.7%
0.5	1.7%	2.7%
1	1.7%	2.7%
2	1.7%	2.7%
3	1.7%	2.7%
5	2.3%	3.0%
6	2.3%	3.0%
10	3.5%	3.0%
15	3.5%	3.0%
20	3.5%	3.0%

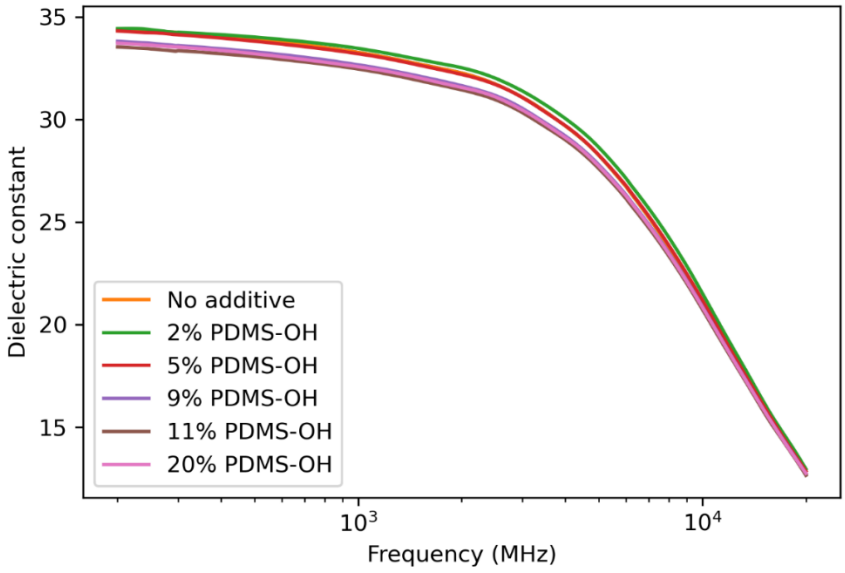

Figure S5 Dielectric constant for the solution with different percentages of PDMS-OH additives.

4. Fiber surface chemistry

The surface elemental composition of electrospun fibers was analyzed by XPS.

Table S3 Surface atomic concentration of electrospun membranes

Additive	Atomic concentration (%)				Theoretical surface Si concentration (%)*
	C	N	O	Si	
-	69.3	3.9	23.0	3.8	0
2 % PDMS-OH	67.4	2.5	24.4	5.7	0.49
5 % PDMS-OH	66.0	1.2	24.0	8.9	1.19
9 % PDMS-OH	61.1	2.0	25.9	11.0	2.07
11 % PDMS-OH	60.0	2.2	25.6	12.2	2.48
20 % PDMS-OH	58.0	1.0	25.9	15.1	4.15

*Calculated for a homogenous mixture

5. Membranes characterization

Scanning electron micrographs were recorded on a Hitachi S-4800 (Hitachi High-Technologies, Canada) at an accelerating voltage of 2 kV and a current flow of 10 µA. In order to reduce charging effects, mats were sputter-coated with 7 nm of Au/Pd (Polaron Equipment, SEM coating Unit E5100, Kontron AG, Switzerland) before imaging.

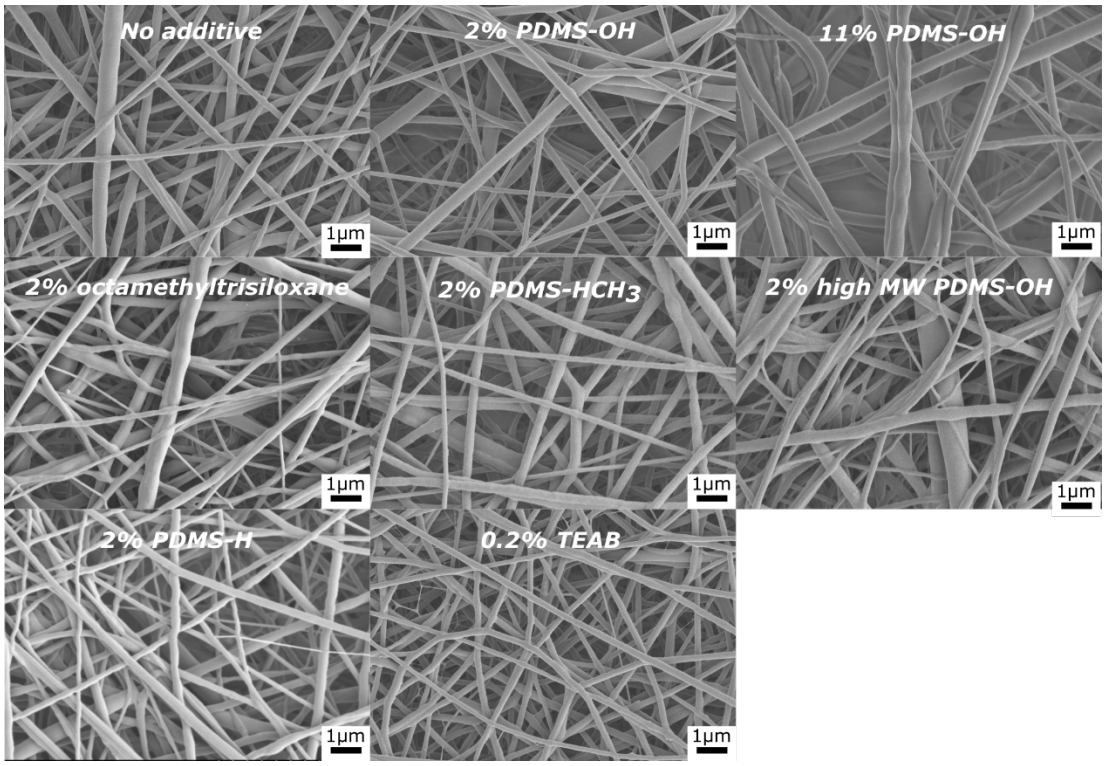

Figure S6 Scanning electron micrographs of electrospun membranes at 10'000x magnification.

6. Jet density calculations

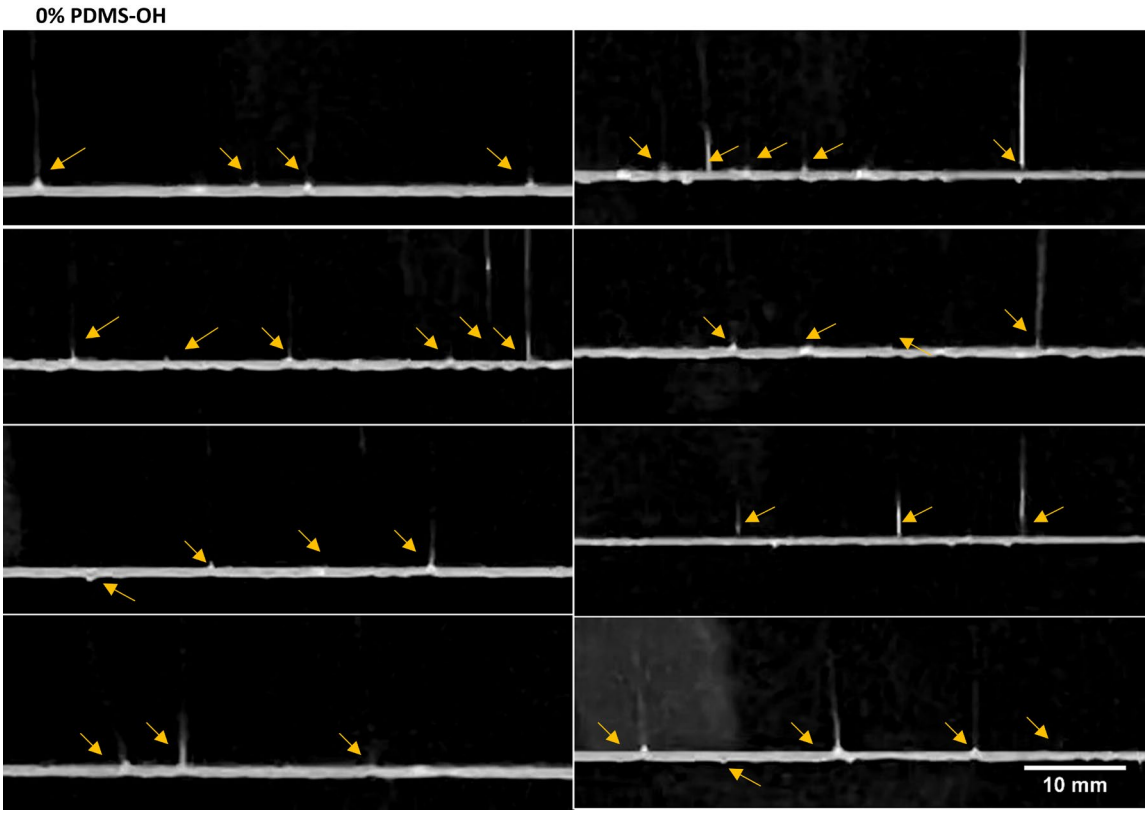

Figure S7 Jet number counting for 0% PDMS-OH additives at 500 ms after carriage leaving the frame with 15 repetitions.

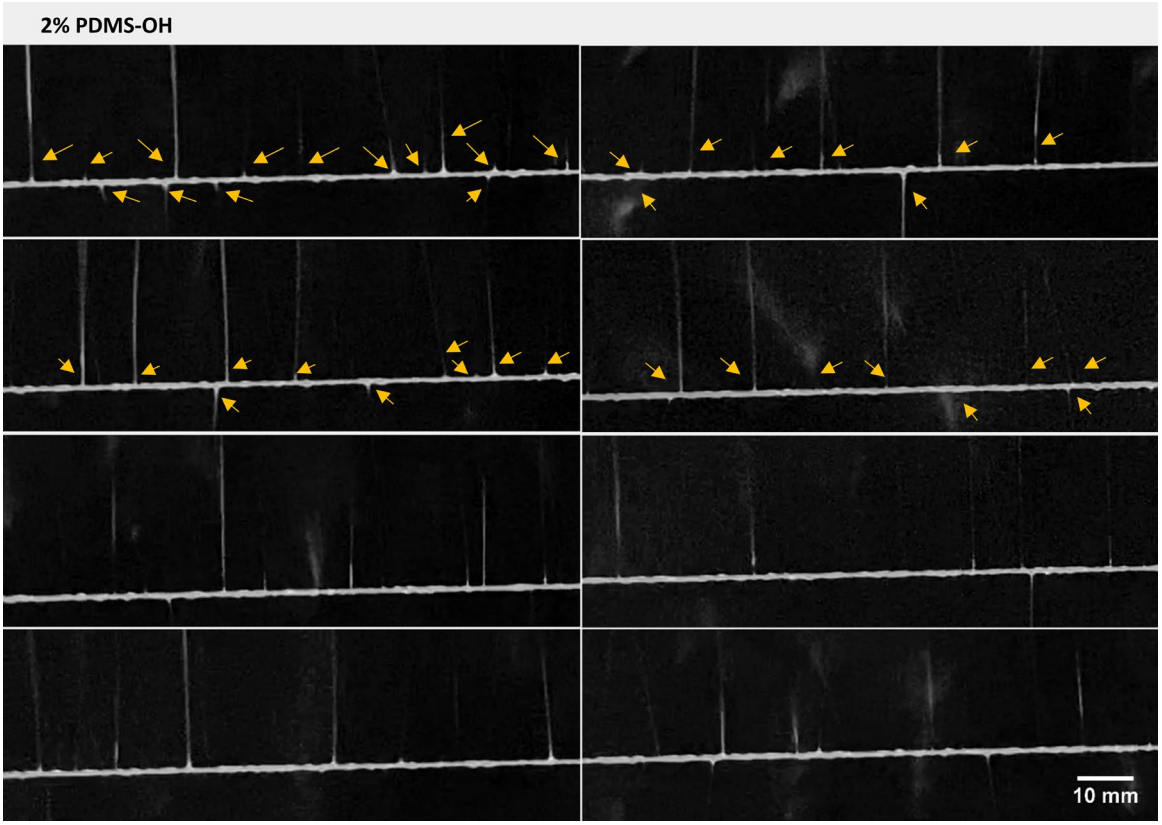

Figure S1 Jet number counting for 2% PDMS-OH additives at 500 ms after carriage leaving the frame with 15 repetitions.

(1) Gregory, A. P.; Clarke, R. N. Dielectric Metrology with Coaxial Sensors. *Meas. Sci. Technol.* **2007**, *18* (5), 1372–1386.

(2) Kaatze, U.; Góttmann, O.; Podbielski, R.; Pottel, R.; Terveer, U. *Dielectric Relaxation in Aqueous Solutions of Some Oxygen-Containing Linear Hydrocarbon Polymers*; 1978; Vol. 82.

(3) Ellison, W. J. Permittivity of Pure Water, at Standard Atmospheric Pressure, over the Frequency Range 0–25THz and the Temperature Range 0–100°C. *J. Phys. Chem. Ref. Data* **2007**, *36* (1), 1–18.